Turkish Journal of Electrical Engineering & Computer Sciences

http://journals.tubitak.gov.tr/elektrik/

Research Article

Turk J Elec Eng & Comp Sci
(2016) 24: 1516 – 1531

doi:10.3906/elk-1307-162

Comparative study of drive systems using vector-controlled PMSM fed by a matrix converter and a conventional frequency converter

Pawel SZCZEŚNIAK[1,*], Konrad URBANSKI[2], Zbigniew FEDYCZAK[1], Krzysztof ZAWIRSKI[2]

[1]Institute of Electrical Engineering, Faculty of Computer, Electrical and Control Engineering, University of Zielona Gora, Zielona Gora, Poland

[2]Institute of Control and Information Engineering, Faculty of Electrical Engineering, Poznan University of Technology, Poznan, Poland

Received: 20.07.2013 • **Accepted/Published Online:** 01.04.2014 • **Final Version:** 23.03.2016

Abstract: This paper presents a comparative study of a drive system with a permanent magnet synchronous motor fed by a matrix converter and a voltage source inverter with diode rectifier stage. A rotor-oriented vector control is implemented in the drive control. Space vector modulation techniques are used for both converters in the output current modulation process. Initial simulation test results and comparison are presented. The advantages of both solutions are indicated. Special attention is given to the drive control in the low speed range. The main aim of this article is to present drive systems with a matrix converter as an interesting alternative solution for automation systems for precision control of speed and position. The technological contribution of this study lies in its potential application to robotics.

Key words: Drive systems, frequency converter, matrix converter, permanent-magnet synchronous motor, space vector modulation

1. Introduction

The permanent-magnet synchronous motor (PMSM) is very popular in various speed control applications for highly efficient industrial drives, robots, process automation, and automobiles. Growing interest may be observed in the PMSM as the best choice of machine in several applications due to its high power density, high torque-to-inertia ratio, small torque ripple and precise control in the low speed range, possibility for torque control at zero speed, high efficiency, and small size [1–5]. The power AC-AC converter is needed for speed and positioning control of the drive system. The converter should also be characterized by high efficiency, small size, and long lifetime. Converter systems with either a voltage or current DC link are commonly used in industrial applications [6]. Such converters are known as indirect frequency converters with a DC energy storage element and have been investigated extensively for many years. An AC-AC converter with bidirectional power flow can be implemented by the coupling of a PWM rectifier and a PWM inverter to the DC link. In this kind of converter, both converter stages, rectification and inversion, are to a large extent decoupled in the control process, which is an advantage. On the other hand, the DC link energy storage element has a relatively large physical volume. Furthermore, in case of the VSI, the application of electrolytic capacitors is a major cause of reduced converter lifetime [6,7]. Recently, the matrix converter (MC) has emerged as an attractive alternative to the conventional AC-AC converter with DC energy storage element [8]. The lack of bulky capacitors, the

*Correspondence: p.szczesniak@iee.uz.zgora.pl

possibility to obtain a unity input power factor, and a bigger choice of voltage vectors are significant advantages of such converters. Furthermore, the MC provides a compact solution for a four-quadrant frequency converter, which produces sinusoidal input and output currents. Thus, MC integration into the motor should also be more reliable than the integration of conventional two-stage converters [7].

To exploit the above presented advantages of the PMSM drive, precise rotor positioning data are necessary for efficient vector control. Vector control allows the attainment of good dynamics and excellent performance, especially during transients, and prevents overload of the motor by controlling the motor currents. Generally, in most variable-speed drive systems, the rotor position data are obtained by a shaft position sensor such as an optical absolute encoder or a resolver [1]. Improvements in estimation algorithms over the last few years have resulted in the development of many sensorless control methods for control of the motor without rotor position measurement devices. In these methods the position and speed of the rotor are estimated [2–5].

In the commonly used PWM VSI with DC energy storage element, vector control is conventionally selected for PMSM drive systems to control speed and torque simultaneously. In this converter only eight voltage vectors are selected to output voltage waveform shaping [6,7]. The level of the DC link voltage is used for performing output current waveforms. The small number of voltage vectors available from the VSI makes the torque-ripple problem more challenging. Alternatively, proposed in this paper, a system with a matrix converter provides a greater choice of switching voltages than a VSI [8–10]. The circuit of the MC basically consists of an array of static power switches connected between the source and load terminals. The basic operating principle is synthesis of the load voltage waveforms and source current waveforms from selected segments of the input voltage waveforms and output current waveforms, respectively [8–10]. These converters are able to construct the output voltage waveforms with a lower input voltage, and subsequently lower voltages can be switched into the PMSM. The output performance is better than that of the classical solution [9].

The main goal of this research was to study the potential for using a MC to feed the PMSM in a closed-loop control system with signal feedback of rotor speed and position. Furthermore, a comparative study was implemented of this drive system with one commonly used in the automation process using the VSI and diode rectifier. Space vector modulation (SVM) of MC output voltages [8,10] and a rotor-oriented control technique of PMSM have been used. Special attention has been given to the drive system performance at low speed [9]. Typical distortion of voltage and current waveforms will be discussed for both converters. The performance has been verified by computer simulation tests in MATLAB Simulink.

Initial results of the research are presented in the paper. The analysis of the MC for applications with PMSM and sensorless control will be the subject of ongoing further research. These preliminary results of closed-loop control are very important in the study of the basic properties of PMSMs fed by a matrix converter with respect to further research on the sensorless control method, and on new power converters called matrix-reactance frequency converters [11,12].

This paper consists of six sections, including the introduction. Section 2 introduces the fundamentals of the matrix converter. Section 3 presents the classical solution for a frequency converter based on a voltage source inverter and diode rectifier. In Section 4 the modeling and control strategy of a PMSM drive system are presented. Section 5 illustrates the simulation results of the presented drive systems and their comparison. Section 6 draws conclusions and also makes proposals for future research work on sensorless control.

2. Fundamentals of the matrix converter

Generally, the MC is a single-stage converter with $(m \times n)$ bidirectional power switches, able to directly connect an m-phase source to an n-phase load [8]. Similarly to classical frequency converters with the DC energy storage element (VSI or CSI) [6,7], the MC structure is also divided into two kinds: a voltage source matrix converter (VSMC) or a current source matrix converter (CSMC). The MC, depending on the kind of power supply – voltage or current character – can work as a VSMC or a CSMC, respectively [11,12]. The VSMC of 3 × 3 switches is the most important from a practical point of view, because it connects three-phase systems to a three-phase load and is dedicated to the typical loads, i.e. induction motors. The basic topology of the VSMC is shown in Figure 1 [8].

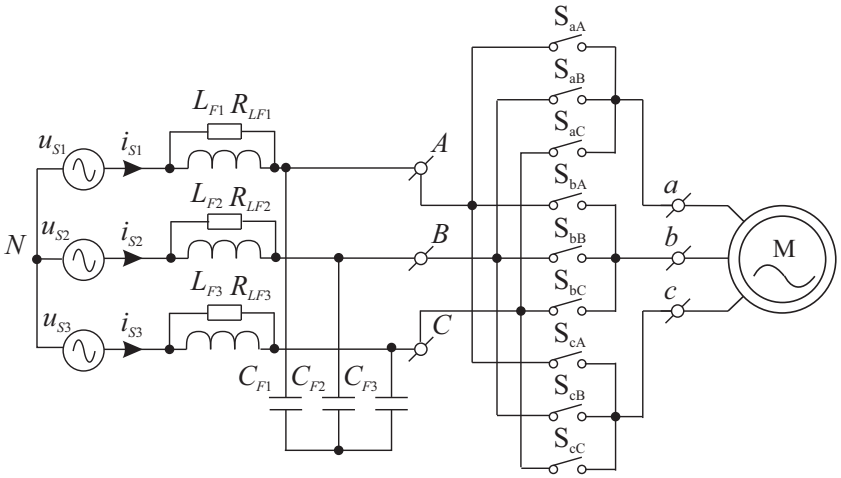

Figure 1. Basic circuit of three-phase voltage source matrix converter.

For high performance, the MC should have a source filter that consists of a second-order LC resonant circuit with a damping resistor in parallel with the inductor [8–10]. The main purpose of the source LC filter is the minimization of the high-frequency components in the input current. The harmonic contents in the input current are close to the switching frequency, and therefore the input filter design of the matrix converter is relatively easy. The filter resonant frequency and damping factor δ are selected from Eq. (1) [8].

$$f_0 = \frac{1}{2\pi\sqrt{L_F C_F}}, \delta = \frac{1}{2R}\sqrt{\frac{C_F}{L_F}} \tag{1}$$

The MC has several modulation strategies that can be applied [8,10,13]. The most used modulation strategy for MCs is space vector modulation (SVM). SVM for MCs is able to synthesize the reference output voltage vector and is also able to control the source current displacement angle [13]. The SVM technique is based on the instantaneous space vector representation of load voltages and source currents in the MC. These representations are defined by the states of its switches S_{jK}. The switching function of a single switch is defined as in Eq. (2) [8]:

$$s_{jK} = \begin{cases} 1, & \text{switch } S_{jK} \text{ closed} \\ 0, & \text{switch } S_{jK} \text{ open} \end{cases}, \tag{2}$$

where $j = \{a,\ b,\ c\}$ is the name of the output phase and $K = \{A,\ B,\ C\}$ is the name of the input phase. Taking into account that the input phases must never be short-circuited and that the output currents must

never be interrupted, the constraints can be expressed as in Eq. (3).

$$s_{jA} + s_{jB} + s_{jC} = 1 \tag{3}$$

With these restrictions, a set of 27 admissible configurations can be recognized, and these combinations are depicted in Table 1. For the SVM of the matrix converter it is convenient to define the following space vectors for each switch configuration [13]:

Table 1. MC switch configurations and vector representations of the line-to-line output voltages and phase input currents in SVM [13].

No.	Vector no.	a	b	c	$\lvert\underline{u}_{OL}\rvert$ [V]	α_{OL}[rad]	$\lvert\underline{i}_{I}\rvert$ [A]	β_I[rad]
1	0_A	A	A	A	0	-	0	-
2	0_B	B	B	B	0	-	0	-
3	0_C	C	C	C	0	-	0	-
4	–3	A	C	C	$u_{CA}2/\sqrt{3}$	$5\pi/6$	$i_a 2/\sqrt{3}$	$-\pi/6$
5	+2	B	C	C	$u_{BC}2/\sqrt{3}$	$-\pi/6$	$i_a 2/\sqrt{3}$	$-\pi/2$
6	–1	B	A	A	$u_{AB}2/\sqrt{3}$	$5\pi/6$	$i_a 2/\sqrt{3}$	$-5\pi/6$
7	+3	C	A	A	$u_{CA}2/\sqrt{3}$	$-\pi/6$	$i_a 2/\sqrt{3}$	$5\pi/6$
8	–2	C	B	B	$u_{BC}2/\sqrt{3}$	$5\pi/6$	$i_a 2/\sqrt{3}$	$\pi/2$
9	+1	A	B	B	$u_{AB}2/\sqrt{3}$	$-\pi/6$	$i_a 2/\sqrt{3}$	$\pi/6$
10	–6	C	A	C	$u_{CA}2/\sqrt{3}$	$\pi/6$	$i_b 2/\sqrt{3}$	$-\pi/6$
11	+5	C	B	C	$u_{BC}2/\sqrt{3}$	$-5\pi/6$	$i_b 2/\sqrt{3}$	$-\pi/2$
12	–4	A	B	A	$u_{AB}2/\sqrt{3}$	$\pi/6$	$i_b 2/\sqrt{3}$	$-5\pi/6$
13	+6	A	C	A	$u_{CA}2/\sqrt{3}$	$-5\pi/6$	$i_b 2/\sqrt{3}$	$5\pi/6$
14	–5	B	C	B	$u_{BC}2/\sqrt{3}$	$\pi/6$	$i_b 2/\sqrt{3}$	$\pi/2$
15	+4	B	A	B	$u_{AB}2/\sqrt{3}$	$-5\pi/6$	$i_b 2/\sqrt{3}$	$\pi/6$
16	–9	C	C	A	$u_{CA}2/\sqrt{3}$	$-\pi/2$	$i_c 2/\sqrt{3}$	$-\pi/6$
17	+8	C	C	B	$u_{BC}2/\sqrt{3}$	$\pi/2$	$i_c 2/\sqrt{3}$	$-\pi/2$
18	–7	A	A	B	$u_{AB}2/\sqrt{3}$	$-\pi/2$	$i_c 2/\sqrt{3}$	$-5\pi/6$
19	+9	A	A	C	$u_{CA}2/\sqrt{3}$	$\pi/2$	$i_c 2/\sqrt{3}$	$5\pi/6$
20	–8	B	B	C	$u_{BC}2/\sqrt{3}$	$-\pi/2$	$i_c 2/\sqrt{3}$	$\pi/2$
21	+7	B	B	A	$u_{AB}2/\sqrt{3}$	$\pi/2$	$i_c 2/\sqrt{3}$	$\pi/6$

$$\underline{u}_{OL} = \frac{2}{3}\left(u_{ab} + \underline{a}u_{bc} + \underline{a}^2 u_{ca}\right) = u_{OL}\left(t\right) e^{j\alpha_{OL}(t)}, \tag{4}$$

$$\underline{i}_{S} = \frac{2}{3}\left(i_A + \underline{a}i_B + \underline{a}^2 i_C\right) = i_S\left(t\right) e^{j\beta_I(t)}, \tag{5}$$

where $\underline{u}_{OL}$ is the space vector representation for the output line-to-line voltage, $\underline{i}_S$ is the space-vector representation for the input phase current, and $\underline{a} = e^{-j2\pi/3}$. The space vectors may be categorized as one of three groups of "zero", "active", and "synchronous" vectors [8,13]. In Figure 2 the output voltage and input current vectors corresponding to the 18 active configurations are shown. The complex space vector plane is divided into six sectors S_O for output voltages and six sectors S_I for source current. The reference output voltage and source current space vectors are constructed by selecting four nonzero configurations, applied for suitable time intervals within the switching sequence period T_{Seq}, as determined by Eqs. (6) and (7) [13]. The zero

configurations are applied to the complete time interval T_{Seq} in Eq. (8):

$$\underline{u}_O = d_I\,\underline{u}_I + d_{II}\,\underline{u}_{II} + d_{III}\,\underline{u}_{III} + d_{IV}\,\underline{u}_{IV}, \tag{6}$$

$$d_k = t_k/T_{Seq}, k = I, II, III, IV, \tag{7}$$

$$d_0 = 1 - d_I - d_{II} - d_{III} - -d_{IV}, \tag{8}$$

where $\underline{u}_I$, $\underline{u}_{II}$, $\underline{u}_{III}$, and $\underline{u}_{IV}$ are the output voltage vectors corresponding to the four selected configurations, and d_I, d_{II}, d_{III}, and d_{IV} are their duty cycles. The "synchronous" vectors of group 3 are not used in SVM.

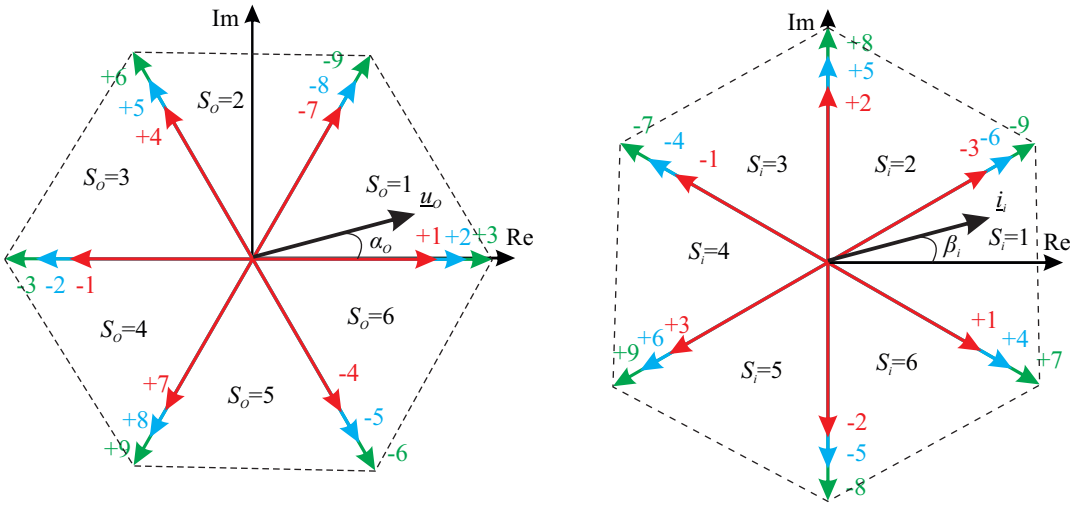

Figure 2. Graphical interpretation of: a) sectors and direction of the output voltage vectors, b) sectors and directions of the input line current vectors.

The required modulation duty cycles for the switching configurations I, II, III, and IV are given by Eqs. (9) through (12) [13]:

$$d_I = (-1)^{S_0+S_i+1}\frac{2}{\sqrt{3}}q\frac{\cos(\alpha_0 - \pi/3)\cos(\beta_i - \pi/3)}{\cos\phi_i}, \tag{9}$$

$$d_{II} = (-1)^{S_0+S_i}\frac{2}{\sqrt{3}}q\frac{\cos(\alpha_0 - \pi/3)\cos(\beta_i + \pi/3)}{\cos\phi_i}, \tag{10}$$

$$d_{III} = (-1)^{S_0+S_i}\frac{2}{\sqrt{3}}q\frac{\cos(\alpha_0 + \pi/3)\cos(\beta_i - \pi/3)}{\cos\phi_i}, \tag{11}$$

$$d_{IV} = (-1)^{S_0+S_i+1}\frac{2}{\sqrt{3}}q\frac{\cos(\alpha_0 + \pi/3)\cos(\beta_i + \pi/3)}{\cos\phi_i}, \tag{12}$$

where φ_i is the input phase displacement angle, and α_O and β_i are the angles of the output voltage and input current vectors measured from the bisecting line of the corresponding sectors and are limited as follows:

$$-\pi/6 < \alpha_0 < \pi/6, \quad -\pi/6 < \beta_i < \pi/6. \tag{13}$$

3. Frequency converter with VSI and diode rectifier

The most traditional AC-AC power converter topology is the pulse width modulated voltage source inverter (PWM-VSI) with a front-end diode rectifier and a DC link capacitor, as shown in Figure 3 [6,14]. The control of the output is achieved by the PWM in the inverter stage so as to produce near sinusoidal output currents in the inductive load, at a desired amplitude and frequency. The source current in this converter is highly distorted, containing high amounts of low-order harmonics (5th and 7th) [14]. Through the impedance of the mains, the low-order current harmonics may distort the voltage at the point of common coupling, which may further interfere with other electric systems in the network. The DC energy storage in the presented indirect frequency converters is a bulky component. In the solution with a VSI the DC link capacitors are relatively large compared to the size of the rectifier and inverter semiconductor components. Electrolytic capacitors typically occupy from 30% to 50% of the total volume of the converter for power levels greater than a few kilowatts, and in addition to this they are a component with a limited lifetime.

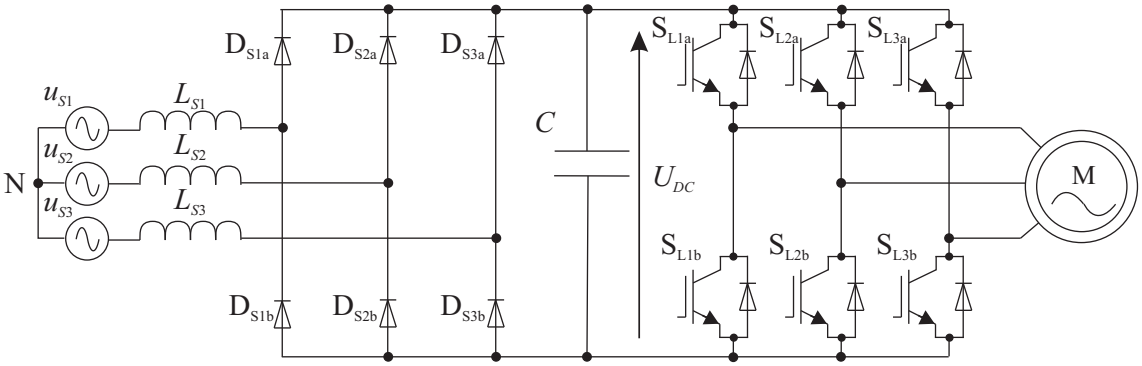

Figure 3. Classical frequency converter with voltage source inverter (VSI) and diode bridge rectifier.

The classical VSI generates a low-frequency output voltage with controllable magnitude and frequency by programming high-frequency voltage pulses. SVM is the commonly used modulation method. In the three-phase VSI each stage is identified as one of eight switch combinations, which are shown in Table 2 [14]. Two of these states are a short circuit of the output terminals while the other six produce active voltages. Each active switch configuration in the VSI corresponds to active space vectors, while the zero configurations correspond to zero space vectors. Active vectors are represented in the complex plane as shown in Figure 4 [14].

Table 2. Switch configurations and corresponding load voltages in the VSI.

No.	S_{L1a}, S_{L2a}, S_{L3a}	S_{L1b}, S_{L2b}, S_{L3b}	u_{L1n}	u_{L2n}	u_{L3n}
1	1 1 0	0 0 1	$1/3U_{DC}$	$1/3U_{DC}$	$-2/3U_{DC}$
2	1 0 0	0 1 1	$2/3U_{DC}$	$-1/3U_{DC}$	$-1/3U_{DC}$
3	0 1 0	1 0 1	$-1/3U_{DC}$	$2/3U_{DC}$	$-1/3U_{DC}$
4	0 1 1	1 0 0	$-2/3U_{DC}$	$1/3U_{DC}$	$1/3U_{DC}$
5	0 0 1	1 1 0	$-1/3U_{DC}$	$-1/3U_{DC}$	$2/3U_{DC}$
6	1 0 1	0 1 0	$1/3U_{DC}$	$-2/3U_{DC}$	$1/3U_{DC}$
7	1 1 1	0 0 0	0	0	0
8	0 0 0	1 1 1	0	0	0

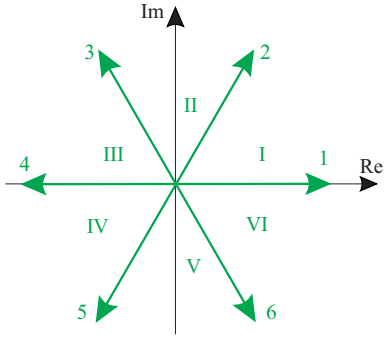

Figure 4. Active stationary vectors on complex plane for three-phase VSI.

4. Modeling and control of PMSM

Simulations were performed using the SimPowerSystems library of the MATLAB Simulink programming environment. As a PMSM, an embedded Simulink model was used. At this level of drive model complexity, such a model is sufficient. The whole system was simulated using various values of the simulation period up to 0.5 μs in step size, depending on the subsystem assignment. All controllers have the proportional integral (PI) structure. Controllers, both for current and speed, have a discrete realization, with a 50 μs calculation step and limited output and integration. The typical setup of the vector control structure with PMSM is shown in Figure 5 [15]. A field-oriented control (FOC) is used due to the following advantages as opposed to DTC [1,16]: low ripple and distortion of the torque and currents (especially important in CNC applications), constant (and smaller in range) switching frequency, and low audible noise emitted in constant frequency. In the control system speed and current controllers are not modified during the test except the frequency converter. As a power source

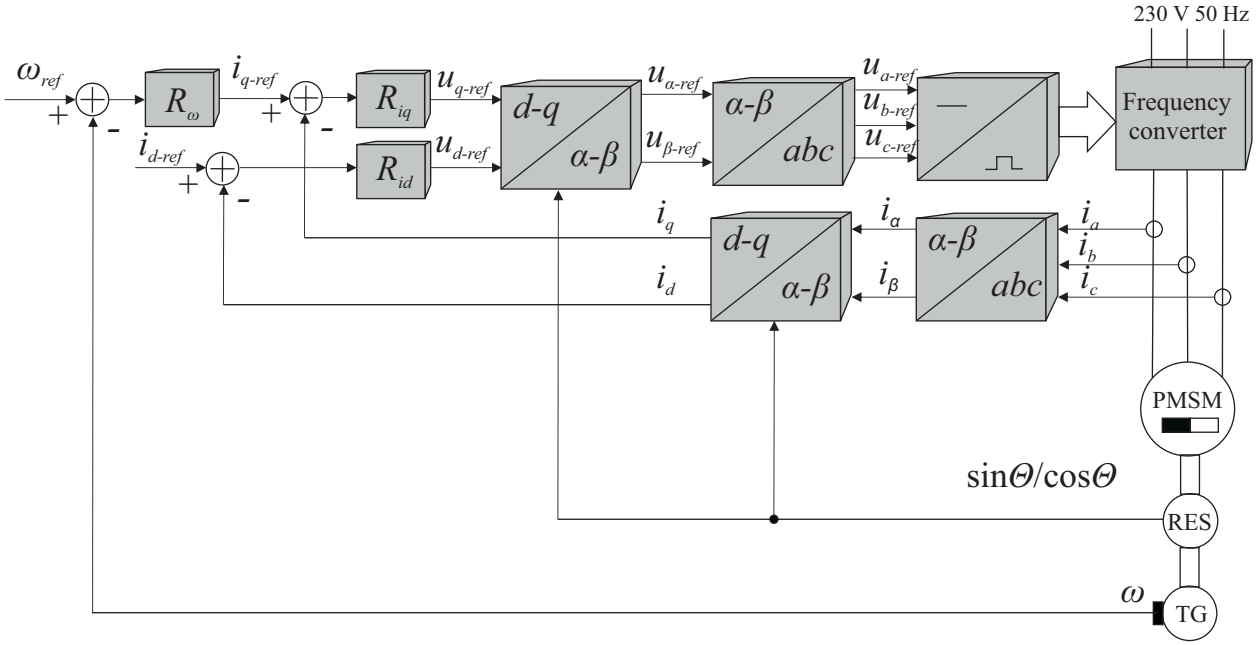

Figure 5. General scheme of the vector control drive system with PMSM.

both the VSI and diode rectifier (Figure 3) and also the MC (Figure 1) are used to perform comparisons. The rotor-oriented vector control system includes a current control loop with dq independent axes (R_{iq} and R_{id} – PI controllers) and outer speed control loop (R_ω – PI controller) [15]. The drive is equipped with a position and a speed sensor.

The parameters of the PMSM are the following:

- phase resistance: 0.7 Ω,
- inductance: 5.7 mH,
- inertia: 0.007273 kg m^2,
- viscous damping: 0.05 N m s.

Only the viscous damping parameter is used for modeling friction. Its value is selected to achieve a load of about 1/3 of the nominal torque for the nominal speed.

5. Simulation results

The system is calculated using a very small simulation period. The fixed-step solver method was used. A step size in the range of 100–500 ns was selected to ensure proper operation. For the medium speed range, a calculation step of 500 ns was used, while in the low speed tests a step of 100 ns was used. The current controller issues a new value every 50 μs and the speed controller every 100 μs. The speed controller settings were the same for tests of both power source configurations.

Selected waveforms are presented in this section. A test of the step response was performed. A test consists of a reference speed change from zero to 100 rad/s in a period of 0.1 s a step change of the motor load from unloaded ($0.4I_{qN}$, where I_{qN} is nominal current in the q axis) to nominal load (Figures 6a and 6b). Figures 7a and 7b present a zoomed part of the transients of acceleration during startup. Because the inverters are modeled accurately using power switches (with PWM including dead time in the VSI), the steady state part of the speed time waveform is not smooth. Generally, the dynamics of both cases cannot be differentiated, but at steady state in a speed, the distortion is visible, especially for the VSI (Figure 7b). The shapes of the motor phase currents, presented in Figures 6a and 6b, do not show any differences in this view, but the effect of the "dead time" for the VSI may be visible when viewed in close-up (Figure 8). The period of 10 ms indicates the dead time phenomena have a significant impact here. It is visible in Figure 8, where the zoomed current waveforms are shown for the zero crossing of phase A at the time of 56 ms. Distortion in phase B and C is noticeable. In the MC the distortion is not visible, because the four-step current-based commutation strategy is used for commutation between two bidirectional switches [9,17].

Figure 9 presents the main difference between both drive systems. In Figure 9a the time waveforms of source currents for the MC are presented, whereas in Figure 9b the time waveforms of source currents for the frequency converter with VSI and diode rectifier are shown. In the drive system with a MC, a sinusoidal-shaped waveform is noticed (Figure 9a). A series of current pulses typical for the diode-based rectifier system are shown in Figure 9b. The benefits of the MC are visible: for the VSI there is a high-value pulse train (loaded motor: about 15 A), but for the MC there is a sinusoidal waveform with maximum value equaling 8 A (under load). A comparison of the spectrum for the line currents is presented in Figure 10. The MC line currents included main components for 50 Hz and harmonic components, which are centered around the switching frequency and its

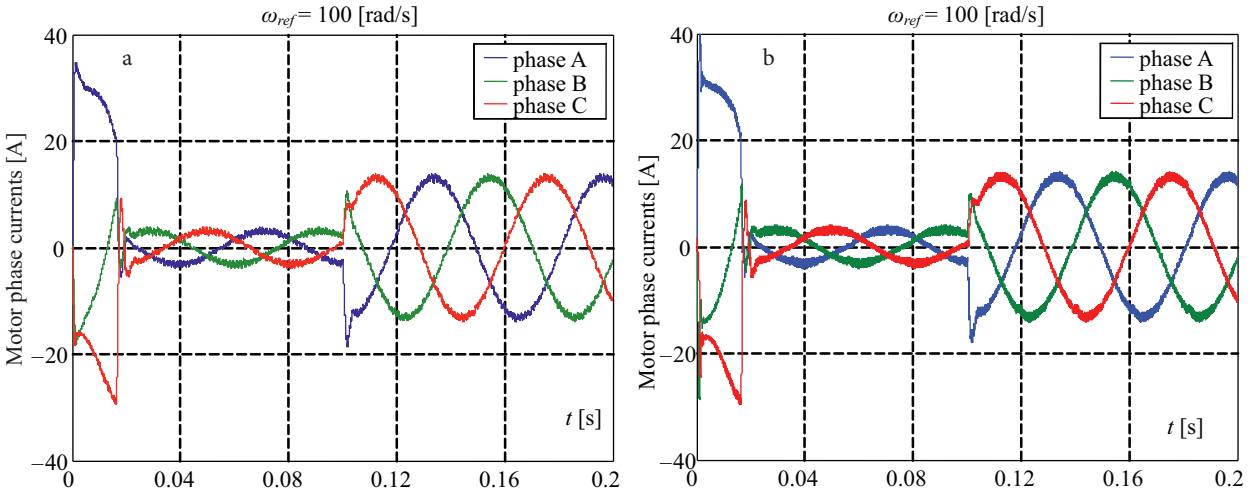

Figure 6. The motor phase currents during test for motor fed by: a) MC, b) VSI.

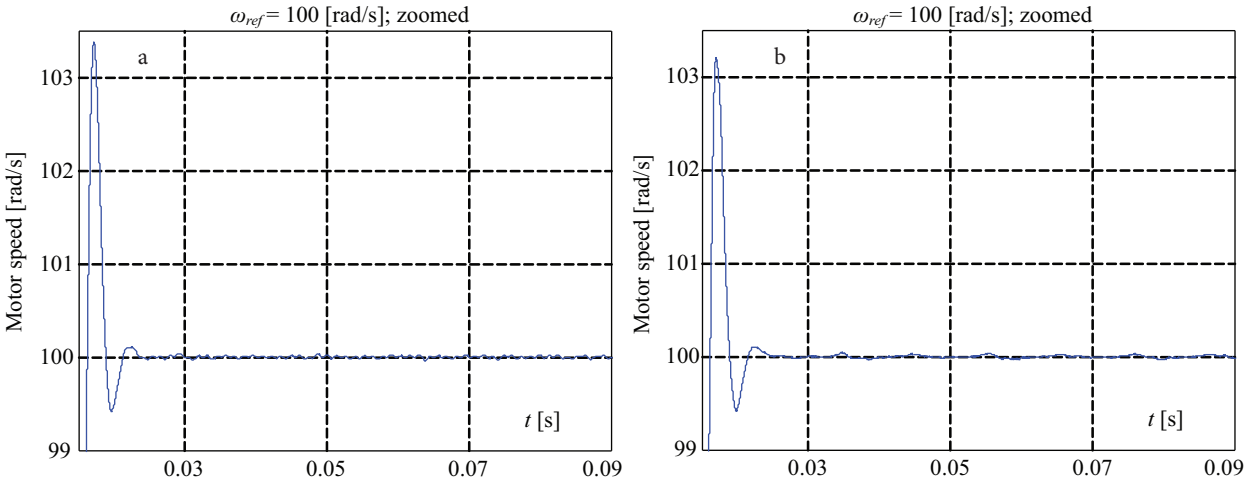

Figure 7. Zoomed part of the speed waveform during startup procedure for motor fed by: a) MC, b) VSI.

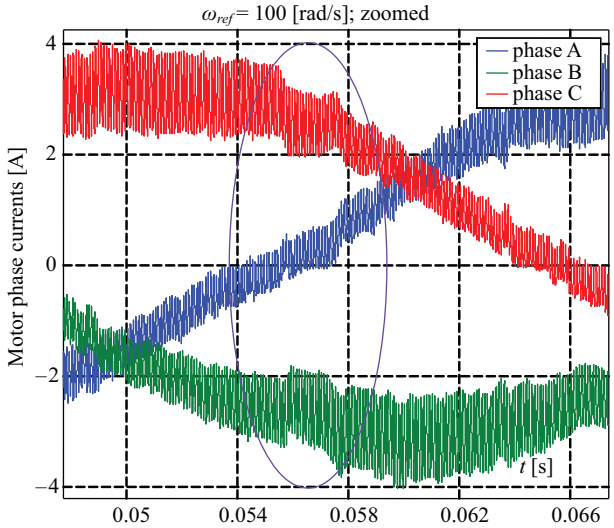

Figure 8. Zoomed part of the motor phase currents for VSI with diode rectifier; at 56 ms zero current crossing distortions are visible.

multiples (20 kHz). In the case of the drive system with diode rectifier and VSI, the source current spectrum consists of low-frequency components at a frequency equaling 50 Hz and its multiples. Figure 10 shows that the MC is a better solution in terms of power quality. This is very important, especially in the case where a large number of converters operate simultaneously, where the source currents are added together. The instantaneous value of source currents can rise to high values.

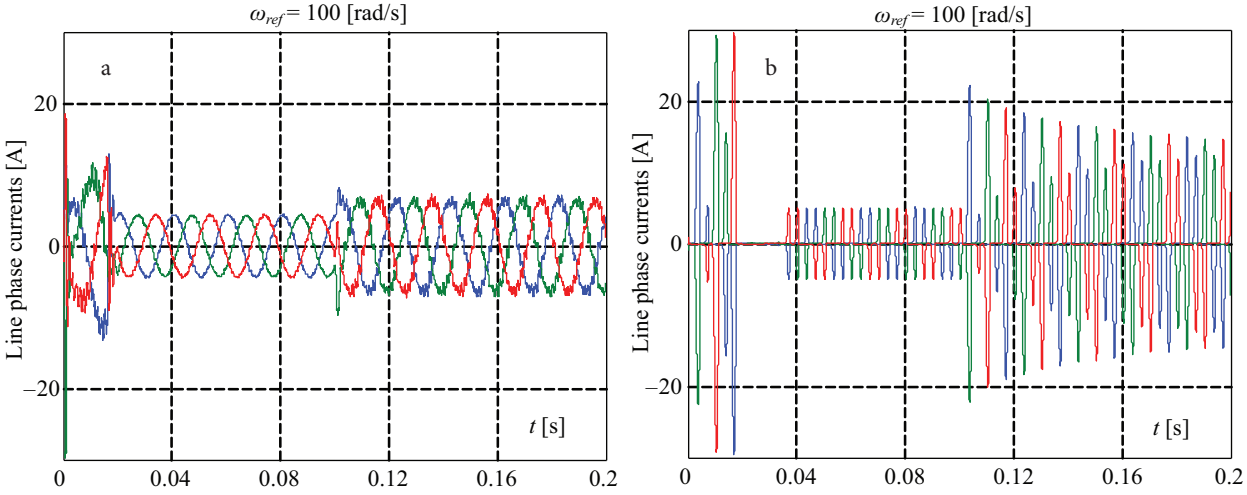

Figure 9. The line currents during test for motor fed by: a) MC, b) VSI.

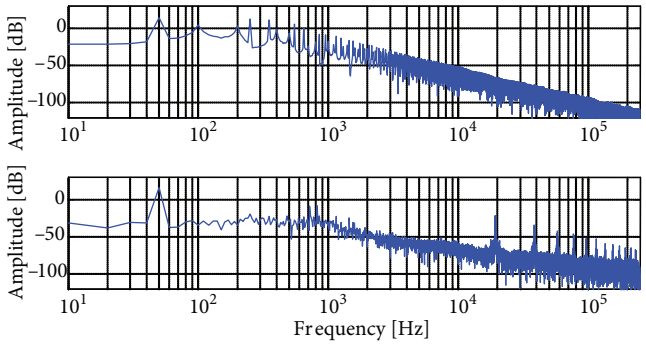

Figure 10. Spectrum of the line currents: a) VSI with diode rectifier, b) MC.

The final test was from startup to a small value of the reference speed equaling 2 rad/s (Figure 11). In the low speed range, where small values of voltage are required, each irregularity in voltage distribution is visible as well as the problems in the low current range with precise set-point tracking. Despite the use of the same controller parameters and reference voltage update period, the set-point tracking quality is much better for the MC (Figure 11a) than the VSI. The VSI model, which includes dead time phenomena, has a significantly worse tracking quality (Figure 11b). The inverter model without dead time phenomena (Figure 11c) gives in the same range of operation a performance worse than that for a MC-based drive. The speed waveforms corresponding to the waveforms from Figure 11 are presented in Figure 12. The oscillation of speed in the VSI with "dead time" is visible.

To conclude this summary, one should note that there are new converters based on the MC, with buck-boost voltage control functionality [11,12]. This solution offers new opportunities to control the speed in dynamic states and stabilize the voltage during instantaneous fluctuations. The selected circuit of such a converter is

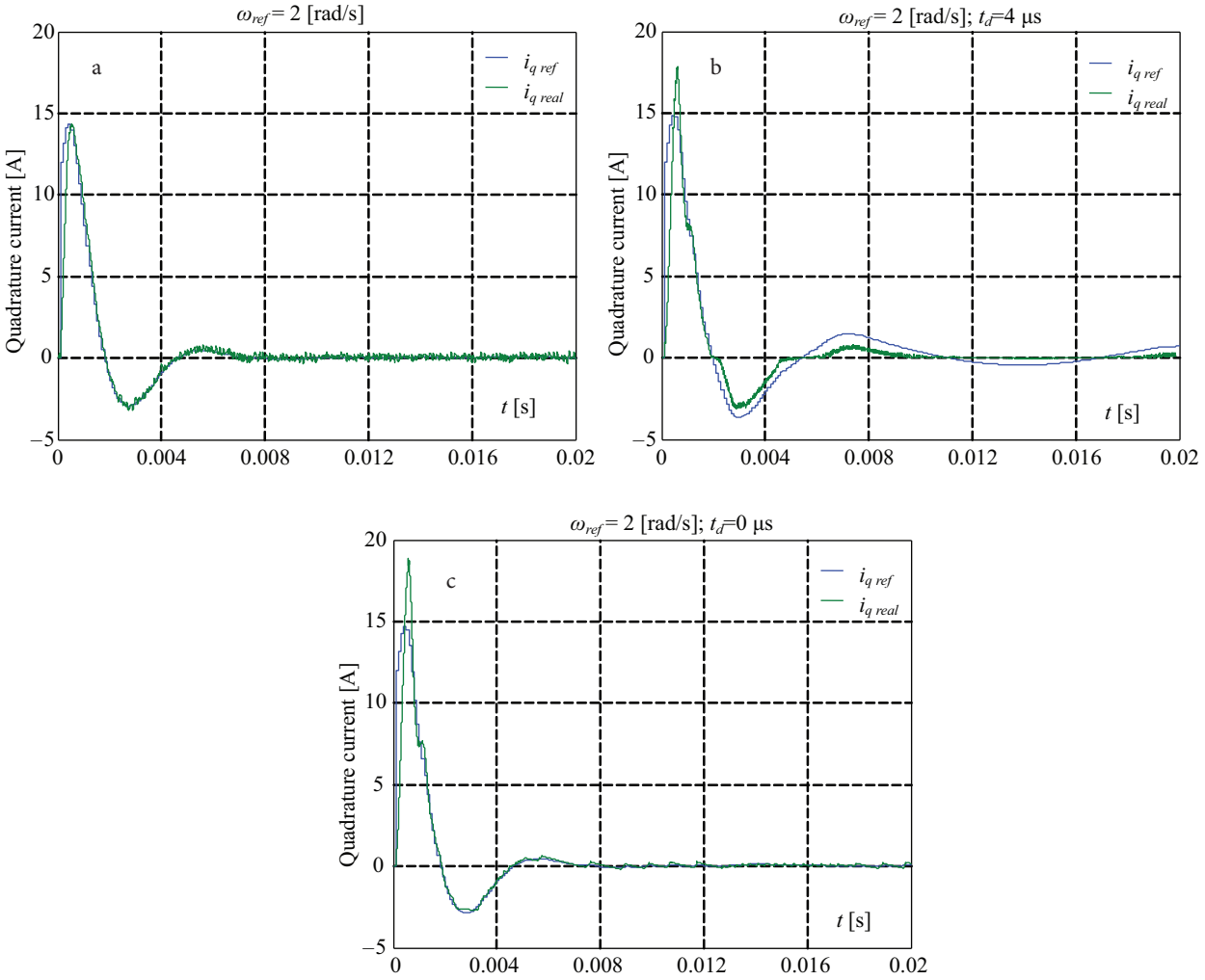

Figure 11. Current waveforms in quadrature axis for the step change of the reference value (0-2 rad/s): a) MC, b) VSI –"dead time" equal to 4 μs, c) VSI – "dead time" equal to 0 μs.

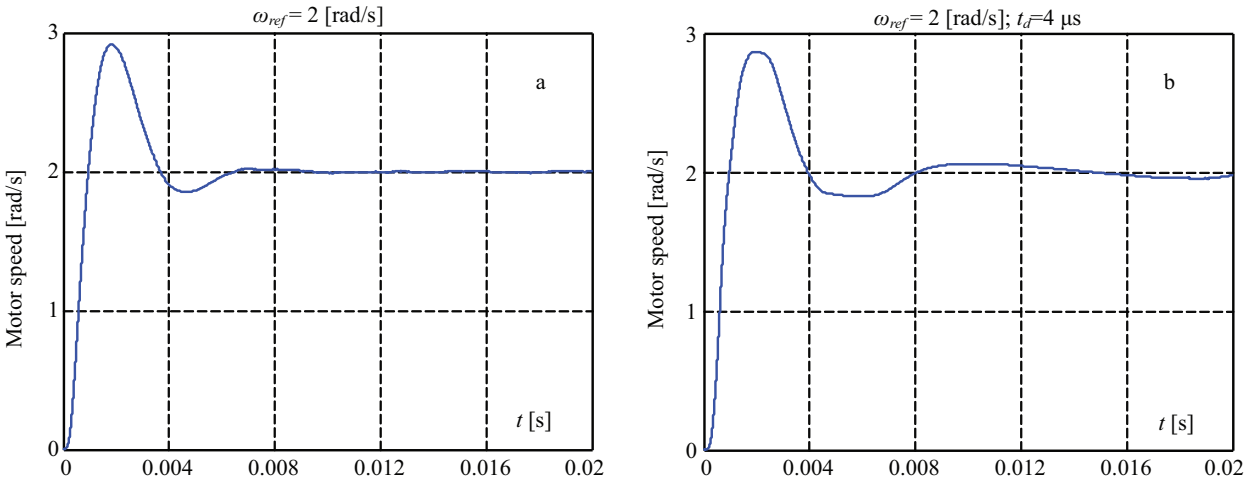

Figure 12. Speed waveforms for the step change of the reference value: a) MC, b) VSI – "dead time" equal to 4 μs, c) VSI – "dead time" equal to 0 μs.

shown in Figure 13. The analysis of such a converter and its potential applications in drive systems will be the subject of ongoing further research.

6. Experimental investigations

Experimental results are presented to confirm the simulations. The experimental setup of a matrix converter prototype, depicted in Figure 14a, consisted of an all-in-one MC configuration prototype module with RB-

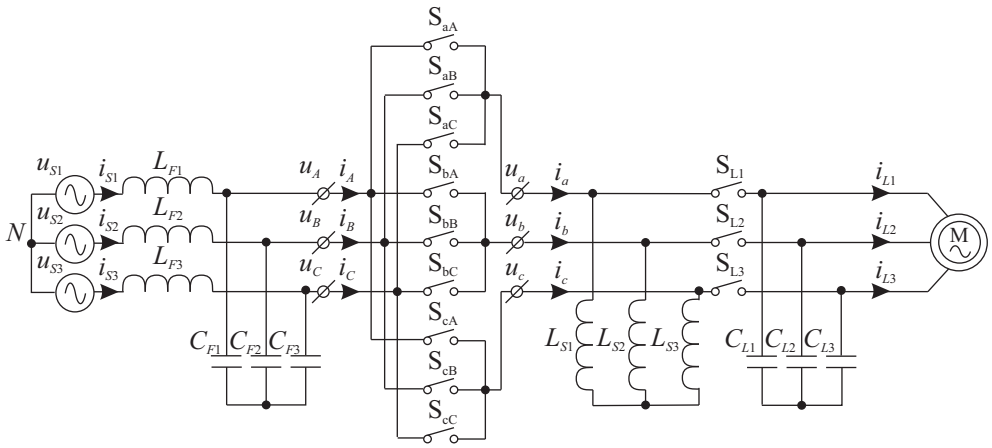

Figure 13. Circuit of three-phase matrix converter with buck-boost topology [11,12].

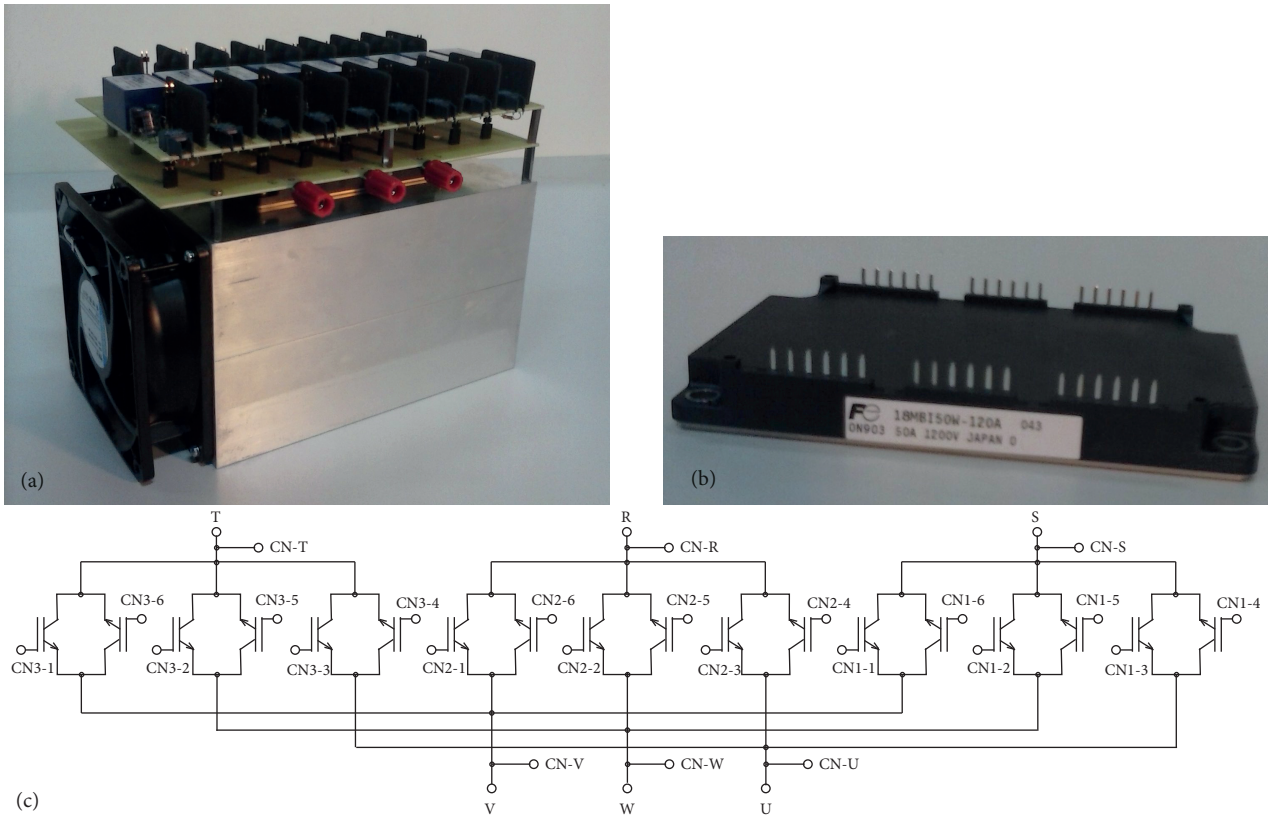

Figure 14. Experimental setup of MC: a) view of the prototype, b) power module of matrix-connected RB-IGBTs, c) topology structure of power module.

IGBTs (1200 V / 50 A), which was introduced by FUJI Electric. A module is shown in Figure 14b, whereas the internal structure is depicted in Figure 14c. The experimental results of a drive system with VSI were obtained from one of the commercially available converters, with a nominal motor power of 1.23 kW. The experimental selected time waveform of system voltages and currents in steady state are presented in Figure 15. The presented comparative study is for illustration only, because the MC prototype was powered by a lower voltage than the nominal value. The obtained results show similar accuracy in the process of motor current control. A detailed quantitative analysis is required in future studies. The source currents of both converters are totally different (Figure 15). The MC current is quasi-sinusoidal with high frequency PWM deformation, whereas for the frequency converter with diode rectifier there are a current pulses. The spectrum analysis of converter source currents is presented in Figure 16. Figure 17 presents some experimental results from the transient state during the startup procedure.

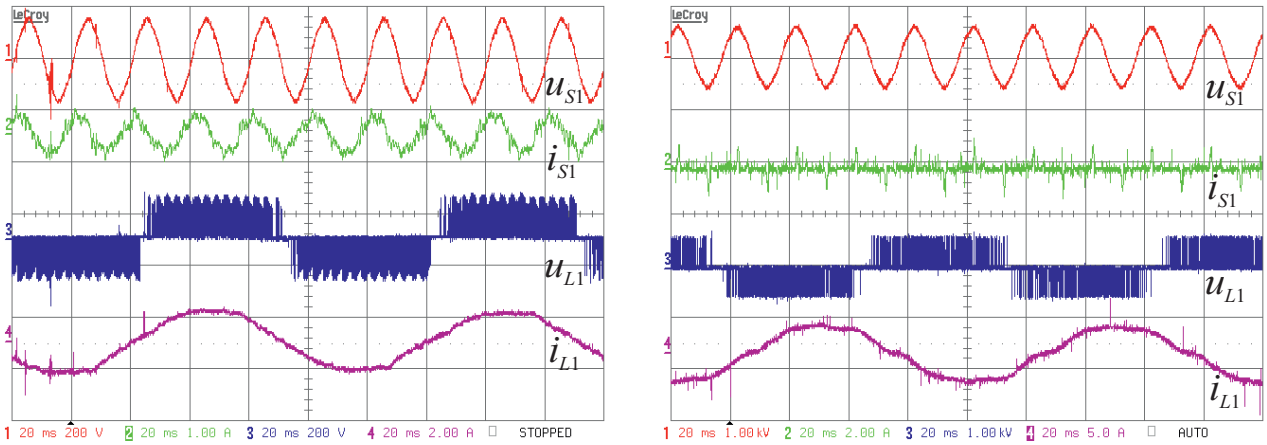

(a) (b)

Figure 15. Experimental time waveforms: a) for MC, b) for VSI with diode rectifier.

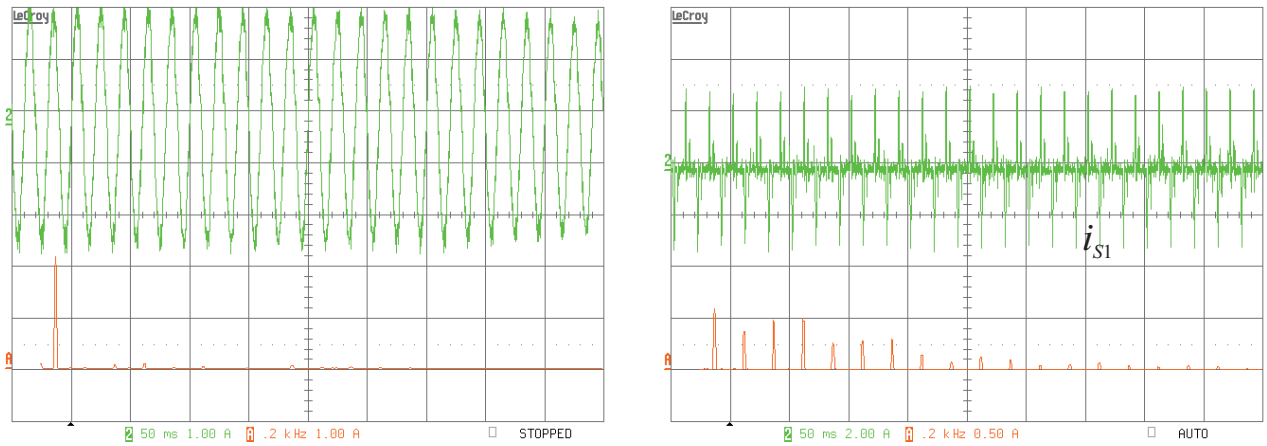

(a) (b)

Figure 16. Spectrum of source current: a) for MC, b) for VSI with diode rectifier.

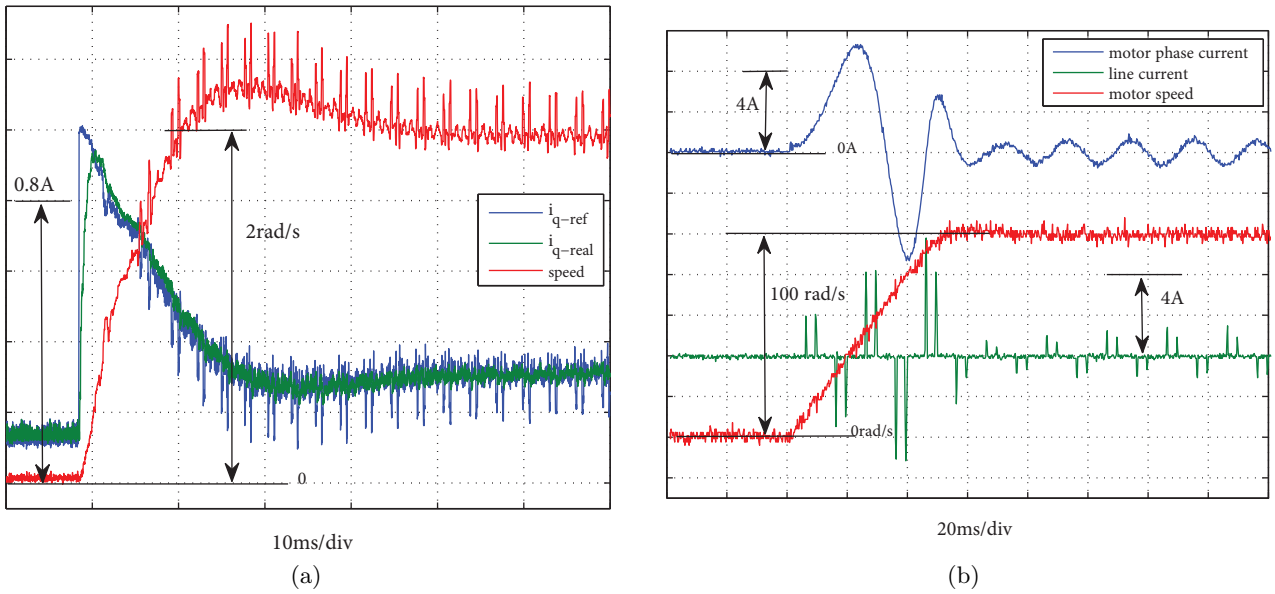

Figure 17. Motor startup process: a) step change of the reference value from standstill to $\omega_{ref} = 2$ rad/s for unloaded motor, b) $\omega_{ref} = 100$ rad/s for unloaded motor.

7. Conclusions

Simulation models are used today to analyze the performance of drive systems fed by different power converters. In this paper, the simulation test results of two drive systems with a PMSM fed by a MC and VSI with diode rectifier (which is most often used in automation applications) have been compared.

Comparison results of the PMSM drive performance presented in the paper indicate the advantages of the MC-fed system. The main advantage of the MC, compared to the VSI with diode rectifier, is the sinusoidal shape of source current waveforms. This kind of frequency converter should be used in particular where an extremely low deformation of the line currents is required. Furthermore, use of the MC may reduce torque ripples caused by dead time phenomena, which are visible in the medium speed range when using a VSI. Another area of operation where the MC shows its supremacy is in the low speed range. The matrix converter enables a more precise elimination of the desired small-value voltage than a typical VSI. With the same reference voltage update period in a MC and VSI, the set-point tracking quality is much better for a MC than a VSI if the drive is operating in a low current range.

Converter systems with a DC link are commonly used in industrial applications. Due to the DC link storage element, an advantage is gained whereby both converter stages, rectification and inversion, are to a large extent decoupled for the control process. On the other hand, the DC link energy storage element has a relatively large physical volume. Furthermore, in the case of the VSI, the application of electrolytic capacitors is a major cause of reduced converter lifetime. The MC topology is an alternative solution to the commonly used VSI with diode rectifier and is characterized by higher performance of output signals, lower volume, lower production costs, and long lifetime (lack of DC link).

Both the presented drive systems were tested using the same controller settings. Similar dynamic properties were achieved for both systems. Taking into account the advantages of the MC compared to a converter with VSI and diode rectifier, the MC is an interesting alternative solution for automation systems for precision control of speed and position.

In this article, experimental results are presented to confirm the simulations. The MC prototype was built based on an RB-IGBT module, which was introduced by FUJI Electric. However, to test the frequency converter with the DC link a commercially available device was used, with a separated control circuit. Generally the experimental test results of the discussed frequency converters confirm the simulation results.

The analysis of MCs for potential applications in drive systems will be the subject of ongoing further research. Such further studies will be focused on the sensorless control algorithm and experimental implementation.

Acknowledgment

The project was funded by the National Science Centre, granted on the basis of decision number DEC-2011/03/B/ST8/06214.

References

[1] Ortega C, Arias A, Caruana C, Balcells J, Asher GM. Improved waveform quality in the direct torque control of matrix-converter-fed PMSM drives. IEEE T Ind Electron 2010; 6: 2101–2110.

[2] Wang Z, Lu Q, Ye Y, Lu K, Fang Y. Investigation of PMSM Back-EMF using sensorless control with parameter variations and measurement errors. Electr Rev 2012; 8: 182–186.

[3] Göksu Ö, Hava AM. Experimental investigation of shaft transducerless speed and position control of ac induction and interior permanent magnet motors. Turk J Electr Eng Co 2010; 5: 865–882.

[4] Urbański K. Sensorless control of PMSM high dynamic drive at low speed range. In: IEEE International Symposium on Industrial Electronics; 27–30 June 2011; Gdansk, Poland. New York, NY, USA: IEEE. pp. 728–732.

[5] Urbański K, Zawirski K. Adaptive observer of rotor speed and position for PMSM sensorless control system. COMPEL 2004; 4: 1129–1145.

[6] Kolar JW, Friedli T, Rodriguez J, Wheeler PW. Review of three-phase PWM AC–AC converter topologies. IEEE T Ind Electron 2011; 11: 4988–5006.

[7] Friedli T, Kolar JW, Rodriguez J, Wheeler PW. Comparative evaluation of three-phase AC–AC matrix converter and voltage DC-link back-to-back converter systems. IEEE T Ind Electron 2012; 12: 4487–4510.

[8] Casadei D, Serra G, Tani A,. Zarri L. A review on matrix converters. Electr Rev 2006; 2: 15–25.

[9] Gao Q, Hua Y, Sumner M, Asher G. Comparison of two sensorless permanent magnet synchronous motor drives fed by a matrix converter and a voltage source inverter using fundamental PWM excitation signals. In: European Power Electronics Conference; 8–10 September 2009; Barcelona, Spain. New York, NY, USA: IEEE.

[10] Rodriguez J, Rivera M, Kolar JW, Wheeler PW. A review of control and modulation methods for matrix converters. IEEE T Ind Electron 2012; 1: 58–70.

[11] Fedyczak Z, Szcześniak P, Korotyeyev I. Generation of matrix-reactance frequency converters based on unipolar PWM AC matrix-reactance choppers. In: IEEE Power Electronics Specialists Conference; 15–19 June 2008; Rhodes, Greece. New York, NY, USA: IEEE. pp. 1821–1827.

[12] Fedyczak Z, Szcześniak P. Matrix-reactance frequency converters using an low frequency transfer matrix modulation method. Electr Pow Syst Res 2012; 1: 91–103.

[13] Casadei D, Serra G, Tani A. Reduction of the input current harmonic content in matrix converters under input/output unbalance. IEEE T Ind Electron 1998; 3: 401–411.

[14] Holmes DG, Lipo YA. Pulse Width Modulation for Power Converters: Principle and Practice. New York, NY, USA: IEEE Press, 2003.

[15] Podlesak TF, Katsis D, Wheeler PW, Clare J, Empringham L, Bland M. A 150 kVA vector controlled matrix converter induction motor drive. IEEE T Ind Appl 2005; 3: 841–847.

[16] Lee HH, Nguyen HM, Chun TW. Implementation of direct torque control method using matrix converter fed induction motor. J Power Electron 2008; 1: 74–80.

[17] Hofmann W, Ziegler M. Multi-step commutation and control policies for matrix converters. J Power Electron 2003; 1: 24–32.